# Charge transport in $Ho_xLu_{1-x}B_{12}$: Separating positive and negative magnetoresistance in metals with magnetic ions

N. E. Sluchanko,[1,2,*] A. L. Khoroshilov,[1,2] M. A. Anisimov,[1] A. N. Azarevich,[1,2] A. V. Bogach,[1] V. V. Glushkov,[1,2] S. V. Demishev,[1,2] V. N. Krasnorussky,[1] N. A. Samarin,[1] N. Yu. Shitsevalova,[3] V. B. Filippov,[3] A. V. Levchenko,[3] G. Pristas,[4] S. Gabani,[4] and K. Flachbart[4]

[1]*A. M. Prokhorov General Physics Institute of RAS, 38 Vavilov Street, 119991 Moscow, Russia*

[2]*Moscow Institute of Physics and Technology, 141700 Dolgoprudnyi, Russia*

[3]*Institute for Problems of Materials Science of National Academy of Sciences of Ukraine, 3 Krzhizhanovskogo Street, 03680 Kiev, Ukraine*

[4]*Institute of Experimental Physics of SAS, 47 Watsonova Street, SK-04001 Kosice, Slovak Republic*

(Received 12 December 2014; revised manuscript received 27 April 2015; published 3 June 2015)

The magnetoresistance (MR) $\Delta\rho/\rho$ of the cage-glass compound $Ho_xLu_{1-x}B_{12}$ with various concentrations of magnetic holmium ions ($x \leqslant 0.5$) has been studied in detail concurrently with magnetization $M(T)$ and Hall effect investigations on high-quality single crystals at temperatures 1.9–120 K and in magnetic field up to 80 kOe. The undertaken analysis of $\Delta\rho/\rho$ allows us to conclude that the large negative magnetoresistance (nMR) observed in the vicinity of the Néel temperature is caused by scattering of charge carriers on magnetic clusters of $Ho^{3+}$ ions, and that these nanosize regions with antiferromagnetic (AF) exchange inside may be considered as short-range-order AF domains. It was shown that the Yosida relation $-\Delta\rho/\rho \sim M^2$ provides an adequate description of the nMR effect for the case of Langevin-type behavior of magnetization. Moreover, a reduction of Ho-ion effective magnetic moments in the range 3–9 $\mu_B$ was found to develop both with temperature lowering and under the increase of holmium content. A phenomenological description of the large positive quadratic contribution $\Delta\rho/\rho \sim \mu_D^2 H^2$ which dominates in $Ho_xLu_{1-x}B_{12}$ in the intermediate temperature range 20–120 K allows us to estimate the drift mobility exponential changes $\mu_D \sim T^{-\alpha}$ with $\alpha = 1.3$–$1.6$ depending on Ho concentration. An even more comprehensive behavior of magnetoresistance has been found in the AF state of $Ho_xLu_{1-x}B_{12}$ where an additional linear positive component was observed and attributed to charge-carrier scattering on the spin density wave (SDW). High-precision measurements of $\Delta\rho/\rho = f(H,T)$ have allowed us also to reconstruct the magnetic $H$-$T$ phase diagram of $Ho_{0.5}Lu_{0.5}B_{12}$ and to resolve its magnetic structure as a superposition of $4f$ (based on localized moments) and $5d$ (based on SDW) components.

DOI: 10.1103/PhysRevB.91.235104 PACS number(s): 72.15.Qm, 72.15.Gd

## I. INTRODUCTION

Magnetoresistance (MR) as a property of a material to change the value of its resistivity in external magnetic field was discovered by Lord Kelvin in 1856 [1], but the mechanisms which are responsible both for negative and positive MR effects in various materials are still a subject of debate [2–10]. Over the past two decades a number of materials with large MR, such as organic semiconductors [10,11], pregraphitic carbon nanofibers, hydrogenated and fluorinated graphene [12–14], amorphous Si doped with magnetic rare-earth ions [15] and bulk germanium doped by multiply charged impurities [16], $SnO_2$ [17], silver chalcogenides [4,18,19], zero-band-gap $Hg_{1-x}Cd_xTe$ [20], and frustrated metallic ferromagnets [21], which are characterized by extreme field sensitivity and/or large values of MR, have been studied in detail, because of their potential for technological applications such as magnetic sensors and/or magnetoresistive reading heads in magnetic recording [22]. Special attention has been paid also to several types of compounds with magnetic $d$ or $f$ ions having "colossal" negative magnetoresistance (CMR) such as manganites [23,24] and cobaltites [25], double perovskites [26], europium-based hexaborides [27], manganese oxide pyrochlores [3,28], Cr-based chalcogenide spinels [29,30], chromium dioxides [31], GdSi [32], MnSi [33], $CeB_6$ and $CeAl_2$ [34,35], and Zintl compound $Eu_{14}MnBi_{11}$ [36], where the MR reaches its largest value near ferro- or antiferromagnetic phase transitions and is quite temperature dependent in this region. Some of the aforementioned compounds are half metals (metallic for one spin orientation of the carriers while insulators for the other orientation); others are degenerate magnetic semiconductors or magnetic metals. At least during the last decade it became evident that colossal magnetoresistance is not exclusive for manganites and debates are emerging that maybe there is some common explanation for these materials beyond (independently of) various structures and/or interactions which characterize each of them. In fact, various types of imperfections (substitution disorder, vacancies and other lattice defects, electronic, magnetic and structural inhomogeneities, nonstoichiometry, phase separation, etc.) can be found in these compounds [11–36]. In particular, in the case of manganites both (i) nanometer-scale coexisting magnetic clusters and (ii) disorder-induced phase separation with percolative characteristics between equal-density phases, together with short-range polaron formation, are the main factors for the dramatic inhomogeneity resulting in a strong influence of external magnetic field and in the appearance of the CMR effect [24]. As a result, it is commonly believed at present that a coexistence of various ordered and disordered phases plays the key role in the CMR effect. Moreover, it is argued that the colossal negative magnetoresistance in compounds with magnetic ions is in fact a Griffiths phase singularity arising in thermodynamic properties at $T_M^{\text{rand}} \leqslant$

*nes@lt.gpi.ru

 

$T \leqslant T_G$, i.e., between the random transition temperature $T_M^{\text{rand}}$ and the "pure" transition temperature $T_G$ [37], and that the vicinity to percolation threshold is the key factor to reach the CMR. In addition, the suppression of short-range static and dynamic polaron correlations in magnetic field is considered as another important component to provide the negative MR effect which dominates in magnetic materials just above $T_M$.

To shed more light on the origin of negative magnetoresistance observed in strongly correlated electron systems at the vicinity of magnetic phase transitions it is useful to investigate model compounds with a quite simple crystalline and magnetic structure where both different types of disorder and a dispersion of size and number of magnetic clusters can be formed and controlled in the vicinity of magnetic phase transition. As promising materials for the study of negative MR effect we have chosen the fcc metallic substitutional solid solutions $Ho_xLu_{1-x}B_{12}$ with Ho magnetic ions embedded in a rigid covalent boron cage of the dodecaboride lattice. Comprehensive investigations of high-quality single crystals of $LuB_{12}$ with various boron isotope compositions allowed recently finding a new disordered "cage-glass" phase at liquid nitrogen temperatures [38–40]. It was shown [39,40] that the combination of loosely bound states of rare-earth ions in the rigid boron sublattice of $RB_{12}$ compounds [Figs. 1(a)–1(c)] together with randomly arranged boron vacancies (with a concentration ~1%–3%) [Fig. 1(d)] leads to a development of lattice instability at intermediate temperatures. As a result, in the range $T < T^{\star} \sim 60$ K metallic $R^{3+}$ ions become frozen in randomly distributed off-center positions inside truncated $B_{24}$ octahedrons [Figs. 1(b)–1(d)]. In the case of solid solutions $Ho_xLu_{1-x}B_{12}$ with magnetic rare-earth ions, there is also Lu to Ho substitutional disorder which interferes with the random displacements (static disorder) of $R$ sites in the metallic cage-glass phase.

In previous magnetoresistance measurements of the nonmagnetic reference compound $LuB_{12}$ and of the antiferromagnetic (AF) $HoB_{12}$ in AF and paramagnetic (P) states a large negative MR effect (of about 30% in magnetic field $H \sim 80$ kOe) was observed in $HoB_{12}$ in the vicinity of the AF-P phase transition [41]. Taking into account that holmium to lutetium substitution in the $Ho_xLu_{1-x}B_{12}$ system is accompanied with Néel temperature lowering from $T_N \approx 7.4$ K for $x = 1$ to $T_N \approx 1.9$ K for $x = 0.3$ [42,43] and that at least for $x \leqslant 0.1$ a paramagnetic ground state is detected in these dodecaborides, it becomes possible to investigate the emergence of the negative MR effect in absence of AF long-range order in diluted magnetic compounds with small nanosize magnetic clusters of Ho ions embedded in the boron matrix [Fig. 1(e)]. Moreover, an infinite magnetic cluster of holmium ions is expected to appear when the $x$(Ho) concentration exceeds the percolation threshold value $x_C$ in the fcc lattice [Fig. 1(f)], which is accompanied by AF ground-state formation in $Ho_xLu_{1-x}B_{12}$ in the range $0.2 < x < 0.3$. It is worth noting that in these metallic fcc compounds with rare-earth magnetic ions and with indirect exchange (RKKY interaction) both nearest neighbors and next-nearest neighbors of Ho ions should be included in magnetic Ho clusters. Thus, the role of different size magnetic clusters during the emergence of large negative MR effect may be investigated in detail in the vicinity of the AF-P phase boundary in these cage-glass metals.

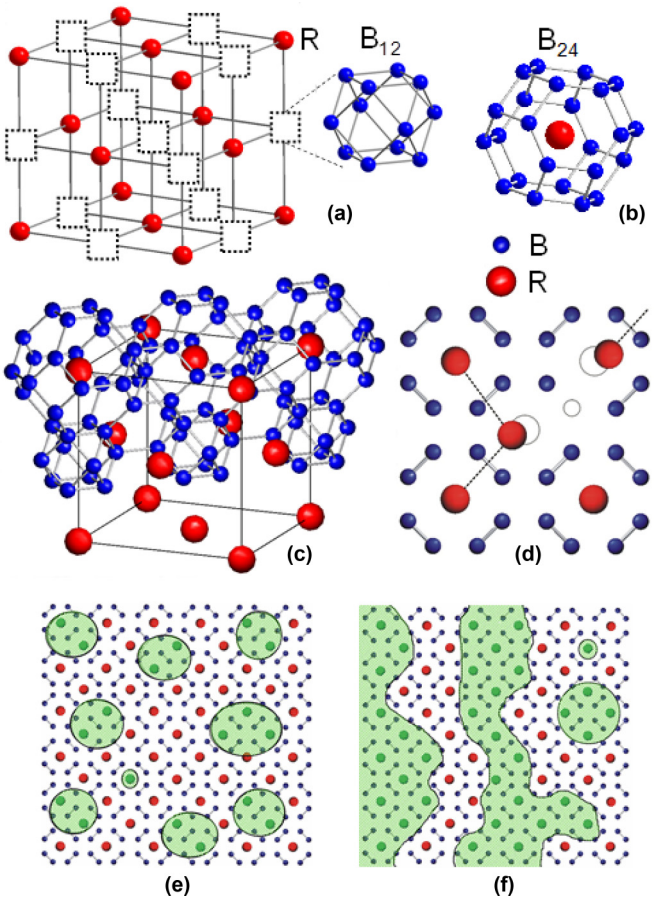


FIG. 1. (Color online) (a) Crystal structure of $Ho_xLu_{1-x}B_{12}$ compounds. The NaCl-type unit cell is built from $R^{3+}$ ions and $B_{12}$ cubo-octahedrons. (b) The first coordination sphere of $R^{3+}$ is arranged as a truncated octahedron $B_{24}$. The arrangement of $R$ and B atoms along the direction ⟨110⟩ and in the (110) section is presented in (c) and (d), respectively. For clarity, $B_{12}$ and $B_{24}$ clusters are shown in (c) only along the upper face diagonal of the lattice. A lattice defect (boron vacancy) is shown (small open circle) in the (110) section (d). Broken $R$-B bonds in the vicinity of the boron vacancy cause displacements of the nearest $R^{3+}$ ions away from the defect by 0.4 Å [51]. As a result, random displacements of the $R^{3+}$ ions, $R^{3+}$ dimers, and other small-size rare-earth clusters [shown in (d)] appear in the $RB_{12}$ matrix. (e) Magnetic clusters of holmium ions in $Ho_xLu_{1-x}B_{12}$ solid solutions in the dilute limit $x \leqslant 0.1$. (f) Formation of infinite magnetic clusters of holmium ions when holmium concentration $x$(Ho) exceeds the value of the percolation threshold $x_C$ (see the text).

The aim of this work was to perform a comparative study of transverse magnetoresistance both for diluted magnetic ($x = 0.01$, 0.04, 0.1, 0.15, and 0.19) and more concentrated antiferromagnetic ($x = 0.23$, 0.3, and 0.5 [42]) $Ho_xLu_{1-x}B_{12}$ solid solutions in the temperature range 1.9÷120 K and in magnetic fields up to 80 kOe. In parallel, we have performed also Hall effect measurements at $H = 80$ kOe for $x = 0.1$ and $x = 0.5$ to compare the drift and Hall mobility of charge carriers, and to clarify the origin of the negative and positive MR components. Additionally, to provide a link between the negative MR and magnetic properties of these model dodecaborides, we have investigated the magnetic

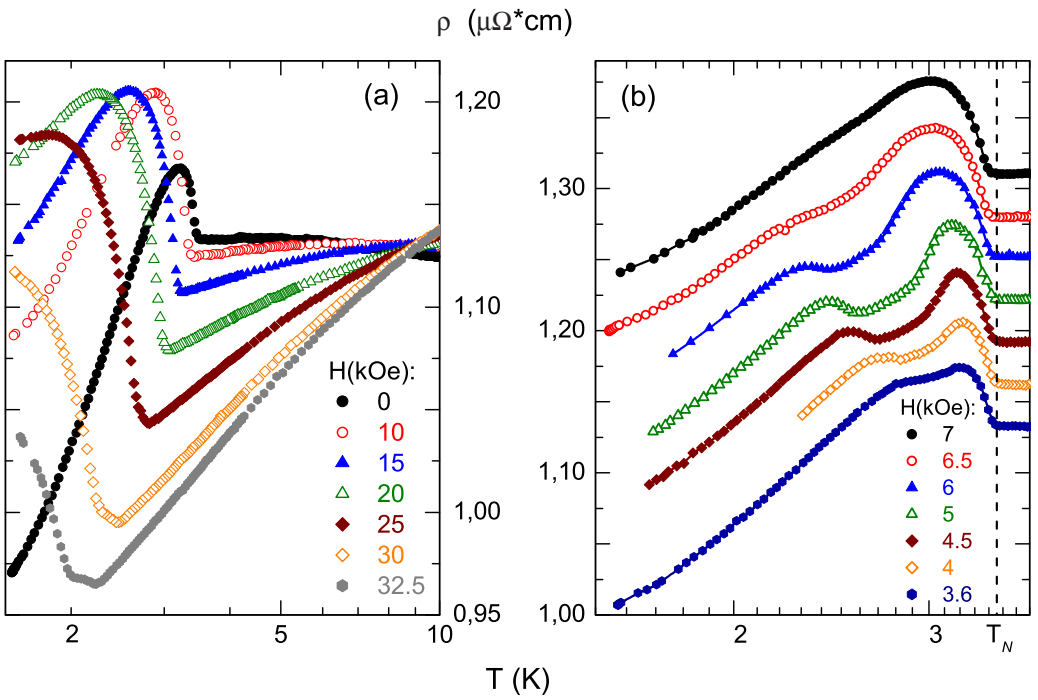


FIG. 2. (Color online) The temperature dependencies of electrical resistivity $\rho(T)$ of the $Ho_{0.5}Lu_{0.5}B_{12}$ compound recorded in magnetic fields $H \leqslant 40$ kOe. In panel (b) the $\rho(T)$ curves are shifted by a constant value 0.3 $\mu\Omega$ cm for convenience.

susceptibility of $Ho_xLu_{1-x}B_{12}$ in a wide temperature range 2–300 K at small magnetic field $H \leqslant 5$ kOe.

We will show in the study that the low-temperature negative magnetoresistance in $Ho_xLu_{1-x}B_{12}$ compounds is attributed to the charge-carrier scattering on magnetic nanodomains and that this negative MR term may be described quantitatively in the framework of relation $-\Delta\rho/\rho \sim M^2_{\rm loc}$ with local magnetization being proportional to the Langevin function for classical moments of the nanosize magnetic clusters of $Ho^{3+}$ ions with AF exchange inside. An additional positive MR component will be also selected and analyzed within the proposed model which is consistent with all received experimental results. However, we cannot exclude other models which might be consistent with these results. Therefore, further experiments (e.g., visualization of magnetic nanoclusters and their real distribution in these magnets) as well as rigorous theoretical work will be needed to receive the definitive description of transport properties in this complex magnetic system of $Ho_xLu_{1-x}B_{12}$ solid solutions.

## II. EXPERIMENTAL DETAILS

In the present study, detailed investigations of resistivity, transverse magnetoresistance, and Hall effect of high-quality single-crystalline samples of $Ho_xLu_{1-x}B_{12}$ solid solutions (see Fig. S1 in the Supplemental Material [69]) with $x = 0.01, 0.04$, 0.1, 0.15, 0.19, 0.23, 0.27, 0.3, and 0.5 were performed in a wide temperature range (1.9 ÷ 120 K) and in magnetic fields of up to 80 kOe ($\mathbf{H}\| \langle 001\rangle$). Resistivity and Hall resistance were measured by the standard dc five-probe technique with the orientation of measuring current $\mathbf{I}\| \langle 110\rangle$. The magnetic susceptibility was measured by a commercial SQUID magnetometer MPMS-5 (Quantum Design). The single crystals used for measurements were grown by vertical crucible-free inductive floating zone melting with multiple re-melting in an inert gas atmosphere on a setup described in detail in [44]. The high accuracy 0.01–0.02 K of temperature control of the sample holder, which was required to perform numerical differentiation of the experimental curves of magnetoresistance $\Delta\rho/\rho = f(H, T_0)$ with respect to magnetic field, was achieved with the help of the commercial temperature controller TC 1.5/300 (Cryotel Ltd.) in combination with a thermometer CERNOX 1050 (Lake Shore Cryotronics, Inc.).

## III. EXPERIMENTAL RESULTS

### A. Resistivity of $Ho_xLu_{1-x}B_{12}$

Figure 2 shows the temperature dependencies of the electrical resistivity $\rho(T)$ of the $Ho_{0.5}Lu_{0.5}B_{12}$ crystal measured in various magnetic fields below 40 kOe in a wider vicinity of the antiferromagnetic-paramagnetic (AF-P) transition. The found Néel temperature $T_N \approx 3.45$ K (Fig. 2) coincides to a good accuracy with results received in [42,43]. As can be seen from Fig. 2, below $T_N$ the resistivity rises to a maximum upon cooling and then decreases with lowering temperature. This is a common behavior of the magnetic part of $\rho(T)$ in metallic magnets with periodic noncollinear spin structures, as observed, e.g., in holmium [45]. With increasing magnetic field the sharp kink at $T_N = 3.45$ K is shifted down to 2 K for $H = 32.5$ kOe [Fig. 2(a)]. This matches the shift of Néel temperature observed in heat capacity data [42] and the magnetic susceptibility results of this compound [43]. The magnetoresistance ratio $\Delta\rho/\rho = [\rho(H) - \rho(H = 0)]/\rho(H = 0)$ for $Ho_{0.5}Lu_{0.5}B_{12}$ is $-19\%$ (negative MR) at 3.45 K and $H = 50$ kOe. Moreover, an additional anomaly in resistivity can be observed just below Néel temperature in low

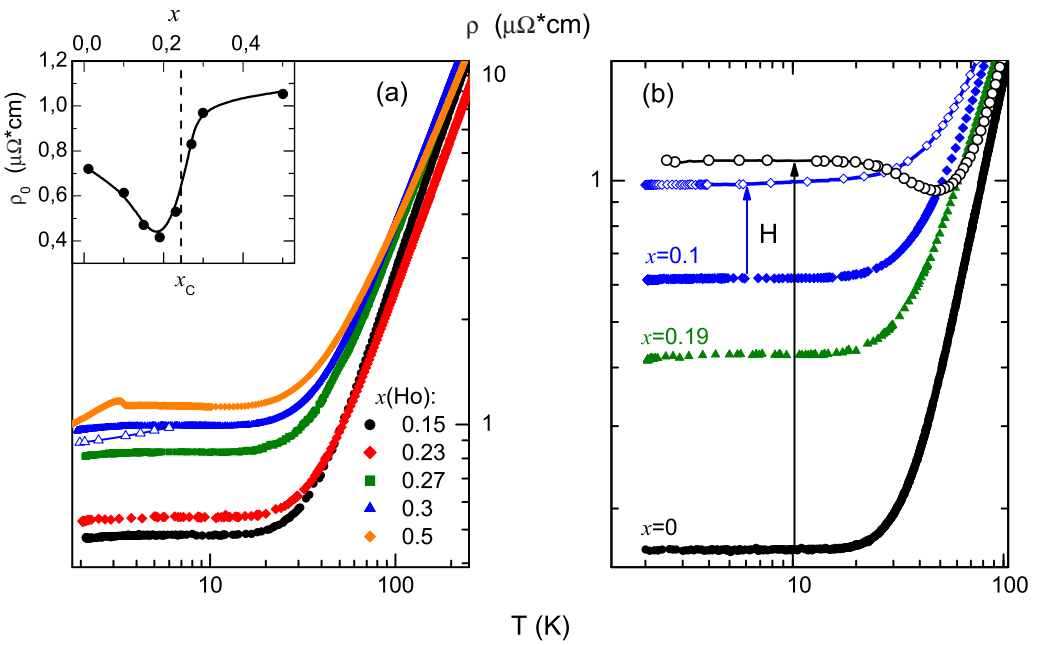


FIG. 3. (Color online) The temperature dependencies of electrical resistivity $\rho(T)$ of solid solutions $Ho_xLu_{1-x}B_{12}$ with $x = 0$, 0.1, 0.15, 0.19, 0.23, 0.3, and 0.5. Additionally presented are data for magnetic fields $H = 30$ kOe [$x = 0.3$, labeled by triangles in panel (a)] and $H = 80$ kOe [$x = 0$, 0.1, labeled by circles and diamonds in panel (b)]. The inset in panel (a) shows the residual resistivity $\rho_0$ versus the holmium concentration $x$ (see the text).

magnetic fields $H < 8$ kOe [Fig. 2(b)] which may be attributed to field-dependent spin-orientation magnetic phase transition, similar to that detected inside the AF phase of $HoB_{12}$ [46].

Figure 3 shows the temperature dependencies of resistivity both for diluted ($x = 0.1$, 0.15, and 0.19) and concentrated ($x = 0.23$, 0.27, 0.3, and 0.5) magnetic $Ho_xLu_{1-x}B_{12}$ solid solutions in the range 1.9–300 K. For comparison, the $\rho(T)$ curve of the nonmagnetic counterpart $LuB_{12}$ (the $4f^{14}$ configuration of the Lu ion corresponds to the case of a completely filled $4f$ shell of the rare-earth ion) is also presented in this

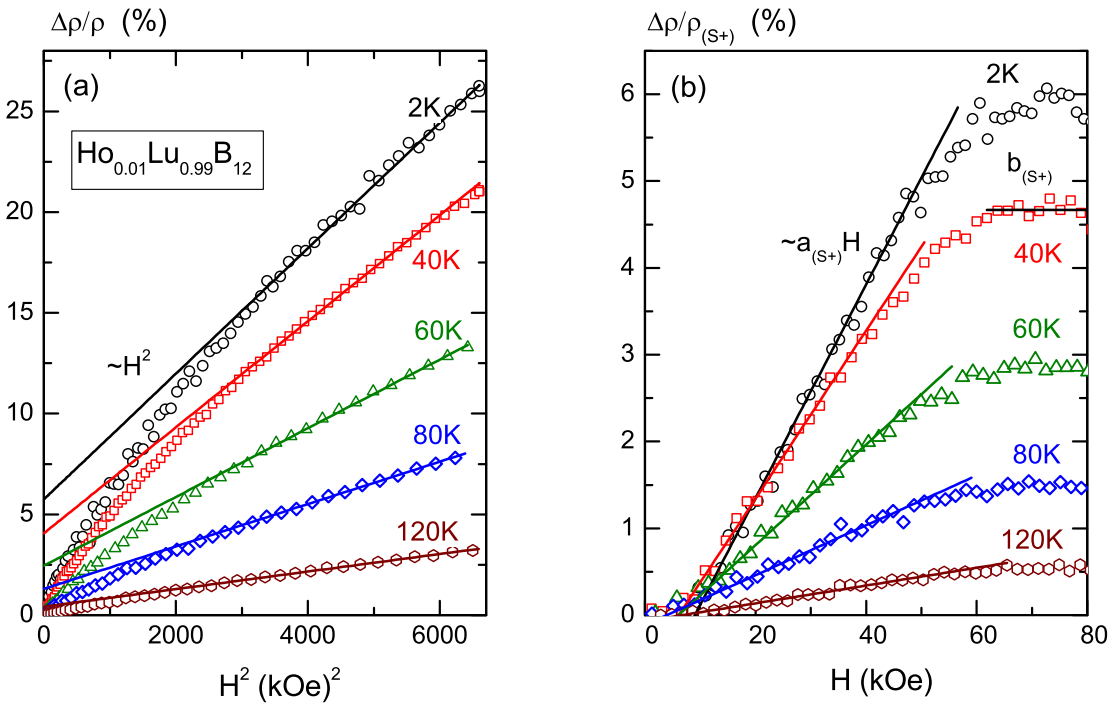


FIG. 4. (Color online) The field dependencies of (a) magnetoresistance in coordinates $\Delta\rho(H)/\rho = f(H^2, T_0)$ and (b) $\Delta\rho(H)/\rho_{(S+)}$ the positive MR component of the $Ho_{0.01}Lu_{0.99}B_{12}$ compound. The solid lines represent the (a) quadratic asymptotic $\sim H^2$ and (b) linear $a_{(S+)}H$ and saturated $b_{(S+)}$ contributions to MR (see the text).

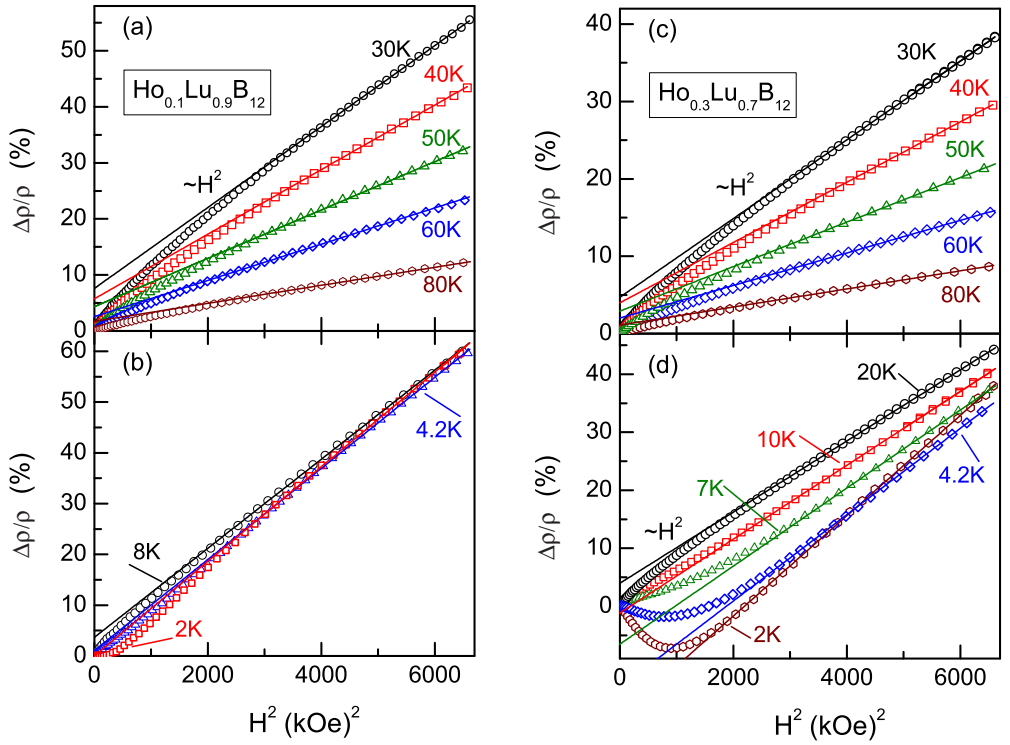


FIG. 5. (Color online) The field dependencies of magnetoresistance in coordinates $\Delta\rho(H)/\rho = f(H^2, T_0)$ of (a), (b) $Ho_{0.1}Lu_{0.9}B_{12}$ and of (c), (d) $Ho_{0.3}Lu_{0.7}B_{12}$ solid solutions. The solid lines in all panels represent the quadratic asymptotic $\sim H^2$.

figure. As can be seen from Fig. 3, all $RB_{12}$ compounds under investigation are good metals, and in the absence of external magnetic field their ratio $\rho(300\,\mathrm{K})/\rho(10\,\mathrm{K})$ exceeds 10 and reaches a maximum value of about 70 for nonmagnetic $LuB_{12}$. In the Ho concentration range $x = 0.04$–$0.19$ the residual resistivity $\rho_0$ decreases in the range 0.4–0.7 $\mu\Omega\,\mathrm{cm}$ (see the inset in Fig. 3), but between $x = 0.23$ and 0.3 $\rho_0$ exhibits a steplike increase with rising Ho concentration, which is supposed to be a consequence of the emergence of an infinite magnetic cluster (percolation) of Ho ions [see Fig. 1(f)], although the $\rho(T)$ behavior does not change considerably (Fig. 3). At intermediate temperatures resistivity can be described by a power-law dependence $\rho(T) \sim T^{\alpha}$ with exponent $\alpha$ varying in the range between 1.3 and 1.7, depending on holmium content. Figure 3 displays also the $\rho(T)$ dependencies of both $LuB_{12}$ and solid solutions $Ho_xLu_{1-x}B_{12}$ with $x = 0.1$ in magnetic field of $H = 80$ kOe, and for $x = 0.3$ at $H = 30$ kOe. It is worth noting that when external magnetic field is applied, the $\rho(T, H = 80\,\mathrm{kOe})$ dependence of $LuB_{12}$ demonstrates an unconventional increase of resistivity with decreasing temperature below the cage-glass transition at $T^{\star} \sim 60$ K (Fig. 3). At the same time, all studied $Ho_xLu_{1-x}B_{12}$ dodecaborides demonstrate a positive magnetoresistance in strong magnetic field. Taking into account that both negative [Fig. 2, $T < 9$ K; Fig. 3(a), curve $H = 30$ kOe for $x = 0.3$] as well as positive [Fig. 3(b), $H = 80$ kOe] MR effects are observed on high-quality single crystals of $Ho_xLu_{1-x}B_{12}$, it appears to be important to measure in detail the magnetic field dependencies $\rho(H, T_0)$ in a wide range of temperatures, to separate and classify the magnetoresistance contributions in these magnetic solid solutions with various holmium content.

### B. Magnetoresistance of $Ho_xLu_{1-x}B_{12}$

Results of MR investigations of $Ho_xLu_{1-x}B_{12}$ solid solutions with a Ho content $x = 0.01$, 0.1, 0.3, and 0.5 are shown in Figs. 4(a), 5(a)–5(b), 5(c)–5(d), and 6(a)–6(d), correspondingly. As can be seen from Fig. 4(a), in the case of the diluted magnetic solid solution $Ho_{0.01}Lu_{0.99}B_{12}$ the magnetoresistance is positive anywhere and demonstrates a strong increase without a tendency to saturation in high magnetic fields up to 80 kOe. With increase of Ho content in the range $x = 0.1$–$0.5$ the aforementioned positive MR effect dominates in the range of intermediate temperatures $T > 20$ K [see Figs. 5(a), 5(c), and 6(a) for $x = 0.1$, 0.3, and 0.5, correspondingly], but below 20 K an emergence of a negative contribution may be observed on $\Delta\rho/\rho(H)$ curves, even for $x = 0.1$ [Fig. 5(b)]. At higher Ho concentration, in the range of $x = 0.19$–$0.5$, a pronounced negative minimum appears on MR vs magnetic field dependencies at liquid helium temperatures [see Fig. 7 and also Figs. 5(d) and 6(b)] and its amplitude and location are strongly dependent on $x$. Indeed, the amplitude of negative MR increases essentially in the range $x = 0.15$–$0.5$ (Fig. 7) where the position of MR minimum changes from $H_{\min}^{MR}(x = 0.15) \sim 16$ kOe to $H_{\min}^{MR}(x = 0.5) \sim 51$ kOe [see also Figs. 5(d) and 6(b)–6(c)]. For comparison, a negative transverse MR with a large amplitude (~20%–30%) was observed previously [41] in the paramagnetic phase of $HoB_{12}$ at temperatures 7.5–15 K. Moreover, the minimum value of negative magnetoresistance in $HoB_{12}$ is expected to be observed in magnetic fields above 80 kOe [41].

The AF-P transition in $Ho_{0.5}Lu_{0.5}B_{12}$ which is, depending on field, observed in the temperature range 1.9–3.5 K, is accompanied by the appearance of an additional

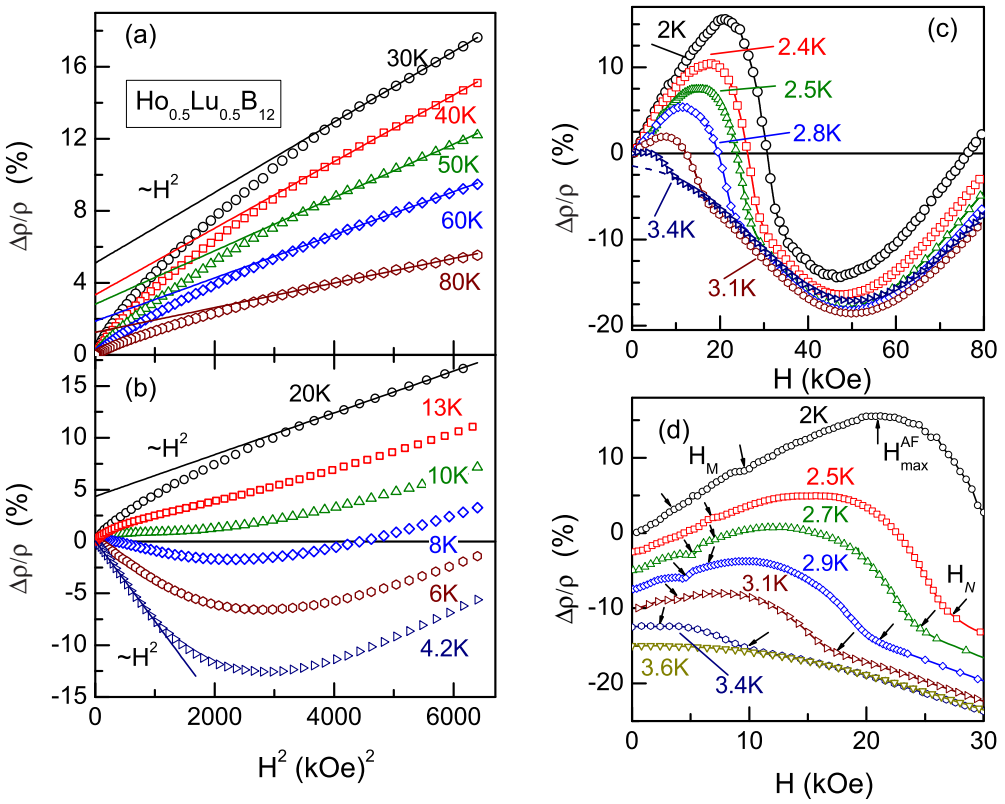


FIG. 6. (Color online) The field dependencies of magnetoresistance in coordinates (a), (b) $\Delta\rho(H)/\rho = f(H^2,T_0)$ and (c), (d) $\Delta\rho(H)/\rho = f(H,T_0)$ of the $Ho_{0.5}Lu_{0.5}B_{12}$ compound. The solid lines in (a) and (b) represent the quadratic asymptotic $\sim H^2$. The $\Delta\rho(H)/\rho$ curves in (d) are shifted by a constant value $\Delta\rho/\rho = 2.5\%$ for convenience. Arrows in (d) indicate the magnetic phase transitions (see the text).

positive antiferromagnetic MR contribution [see Fig. 2 and Figs. 6(c)–6(d)] which becomes fully suppressed by external magnetic field when $H$ reaches the critical values $H_N(T_N)$ on the AF-P phase boundary [Fig. 6(d)]. This additional positive MR component can be attributed to charge-carrier scattering on the magnetic structure in the AF phase of $Ho_{0.5}Lu_{0.5}B_{12}$. A similar positive magnetoresistance was observed previously in the AF phases of $HoB_{12}$, $ErB_{12}$, and $TmB_{12}$ dodecaborides [41] and in antiferromagnetic solid solutions $Tm_{1-x}Yb_xB_{12}$ with $x \leqslant 0.1$ [47]. The mechanism which is responsible for this effect will be discussed below.

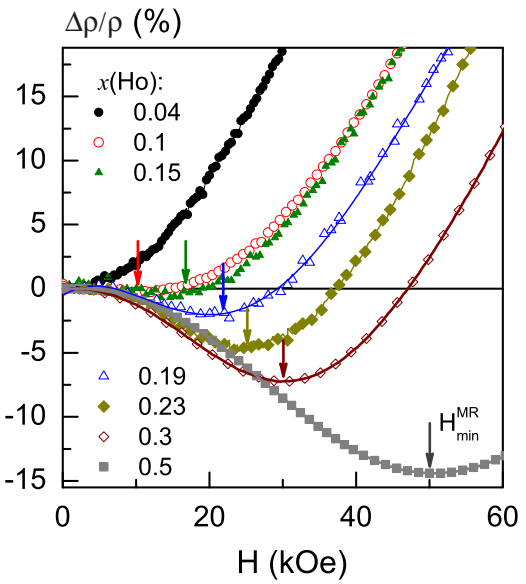


FIG. 7. (Color online) The field dependencies of magnetoresistance of solid solutions $Ho_xLu_{1-x}B_{12}$ with $x = 0.04$, 0.1, 0.15, 0.19, 0.23, 0.3 ($T_0 = 2$ K), and 0.5 ($T_0 = 3.6$ K). The arrows indicate the positions of pronounced negative minima on MR data.

### C. Hall effect and magnetic susceptibility

Figure 8(a) displays results of Hall effect measurements that have been carried out simultaneously with magnetoresistance on several crystals of $Ho_xLu_{1-x}B_{12}$ at magnetic field $H =$ 80 kOe. A pronounced increase (by 15%–25%) of the amplitude of negative Hall coefficient is observed with temperature lowering in the range above the cage-glass transition $T^\star \sim$ 60 K for all studied Ho contents $x = 0.1$ and 0.5 [Fig. 8(a)]. Then, only moderate increase of the absolute values of $R_H(T)$ can be observed with temperature lowering below $T^\star$ for the $Ho_xLu_{1-x}B_{12}$ compound with $x = 0.1$ [Fig. 8(a)]. But on the contrary, for the most concentrated magnetic dodecaboride with $x = 0.5$ non-monotonous behavior with a moderate elevation of the negative $R_H(T)$ is observed at $T_{max} < T < T^\star$ and a smooth maximum appears at $T_{max} \sim 25$ K. A similar strong-field maximum of negative Hall coefficient was found at 20 K in [48] for $HoB_{12}$.

The magnetic susceptibility $\chi(T)$ dependencies received in the present study in small magnetic fields $H = 0.1$ kOe (for

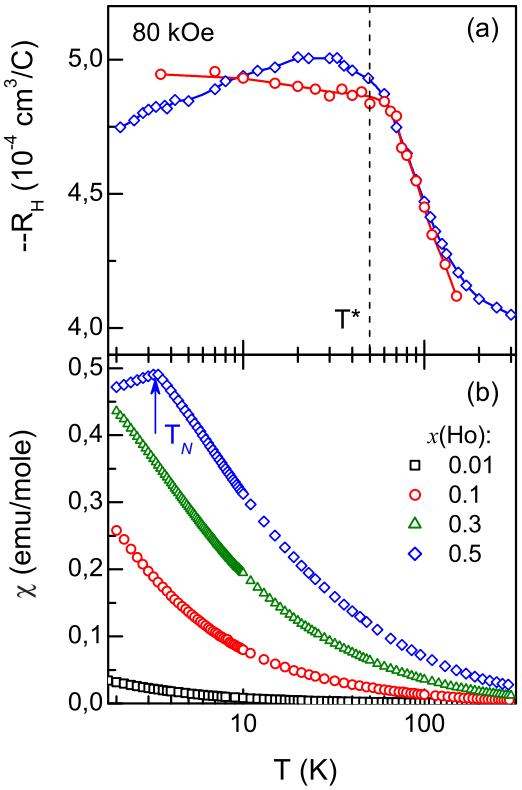


FIG. 8. (Color online) The temperature dependencies of (a) negative Hall coefficient $-R_H(T)$ and (b) magnetic susceptibility $\chi(T)$ of solid solutions $Ho_xLu_{1-x}B_{12}$ with $x = 0.01, 0.1, 0.3$, and 0.5 (squares, circles, triangles, and diamonds, respectively).

$x = 0.1$, 0.3, and 0.5) and in $H = 5$ kOe (for $x = 0.01$) at temperatures in the range 2–300 K are shown in Fig. 8(b). The $\chi(T)$ dependencies demonstrate a paramagnetic Curie-Weiss-type behavior, and for $Ho_xLu_{1-x}B_{12}$ solid solution with $x = 0.5$ the AF-P phase transition is observed at $T_N \approx 3.45$ K [Fig. 8(b)].

In the further analysis and discussion of these results it will be shown that it is possible to separate and classify the aforementioned positive and negative contributions to magnetoresistance. Moreover, the developed approach will demonstrate that the MR components may be estimated quantitatively and that parameters extracted from the data will allow us to describe both the temperature dependence of drift mobility and the characteristics of nanosize magnetic clusters (domains with AF-type short-range order) which are composed from interconnected $Ho^{3+}$ ions embedded in the rigid covalent cage of boron atoms.

## IV. DISCUSSION

To separate and characterize analytically the large negative magnetoresistance effect observed in vicinity of the AF-P transition in $Ho_{0.5}Lu_{0.5}B_{12}$ (Fig. 2) it is first necessary to analyze several positive MR components which are dominant (i) at intermediate temperatures $20 \div 120$ K and (ii) in the antiferromagnetic state of $Ho_xLu_{1-x}B_{12}$ compounds. The most effective approach here is based on investigations of the positive MR in the paramagnetic state of diluted $Ho_xLu_{1-x}B_{12}$ solid solutions (with a small concentration of magnetic impurities $x = 0.01$ and 0.1). From the side of percolation threshold [see inset in Fig. 3(a)], for $x = 0.3$ and 0.5, a large negative MR component appears at low temperatures ($T_N \leqslant T \leqslant 10$ K) versus the positive MR background, and these terms should be analyzed in combination with each other. In the approximation of several additive processes in the scattering of charge carriers in $Ho_xLu_{1-x}B_{12}$, we will gradually develop a phenomenological approach to separate the MR contributions, and then propose the interpretation of the large negative magnetoresistance. We will demonstrate that the large negative MR effect may be explained by scattering of charge carriers on the small-size magnetic clusters of Ho ions, and the Yosida-type relationship $-\Delta\rho/\rho \sim L^2(H/T)$ ($L$ is the Langevin function) will provide us with a good-quality approximation of the negative magnetoresistance behavior. Simultaneously, the analysis of MR in the AF phase will allow us to conclude in favor of a combination of $5d$ and $4f$ components which interplay with each other in the formation of the complicated magnetic structure of $Ho_{0.5}Lu_{0.5}B_{12}$.

### A. Positive magnetoresistance in the paramagnetic phase of $Ho_xLu_{1-x}B_{12}$

Both the MR data presented in coordinates $\Delta\rho/\rho = f(H^2, T_0)$ [see solid lines in Figs. 4(a), 5(a), 5(c) and 6(a), 6(b)] and their numerical derivatives $d(\Delta\rho/\rho)/dH = f(H, T_0)$ (see Fig. S2 in the Supplemental Material [69]) reveal that the positive magnetoresistance observed at intermediate temperatures in high magnetic fields 50–80 kOe follows the quadratic field dependence $\Delta\rho/\rho_{(m+)} = \mu_D^2 H^2$, where from conventional approaches the parameter $\mu_D$ may be considered as the reduced drift mobility of charge carriers. Additionally to this dominant quadratic term $\Delta\rho/\rho_{(m+)}$, there is another positive component $\Delta\rho/\rho_{(s+)}$ detected in a moderate magnetic fields. This second positive MR contribution may be singled out at intermediate temperatures by subtracting the strong-field term $\Delta\rho/\rho_{(m+)} = \mu_D^2 H^2$ from the observed experimental $\Delta\rho/\rho(H)$ dependence. The final $\Delta\rho/\rho_{(s+)}$ is shown, for example, in Figs. 4(b) and 9(a), 9(b) for holmium content $x = 0.01$ and 0.1, respectively. It can be seen from these figures that the second term is negligible in small magnetic fields $H \leqslant 5$ kOe, but it demonstrates an approximately linear field dependence $\Delta\rho/\rho_{(s+)} \sim a_{(s+)}H$ in the range of 10–40 kOe. Then it saturates at high magnetic fields [Figs. 4(b), 9(a)] and its amplitude $b_{(s+)}$ does not exceed 9% at $T > 7$ K for all $Ho_xLu_{1-x}B_{12}$ crystals studied. Moreover, in the case of the diluted magnetic system $Ho_{0.01}Lu_{0.99}B_{12}$ the magnetoresistance exhibits only these two positive contributions both at intermediate and liquid helium temperatures [Fig. 4(b)]. In the absence of the negative MR the analysis of two positive terms $\Delta\rho/\rho_{(m+)}$ and $\Delta\rho/\rho_{(s+)}$ allows us to deduce the temperature dependencies of the above-mentioned coefficients $\mu_D$, $a_{(s+)}$, and $b_{(s+)}$ for $x = 0.01$, and also for $x \geqslant 0.1$ in the range $T >$ 10 K. The resulting $\mu_D(T)$ dependence acquired directly from data of Figs. 4–6 and Fig. 9 is shown in Fig. 10(a). Additionally, Fig. 10(b) shows for comparison the high-field Hall mobility $\mu_H(T) = R_H(T)/\rho(T)$ for $Ho_xLu_{1-x}B_{12}$ with $x = 0.1$ and 0.5. It can be seen that the behaviors of reduced drift $\mu_D$ and Hall $\mu_H$ mobility at $H = 80$ kOe are similar to each other, and

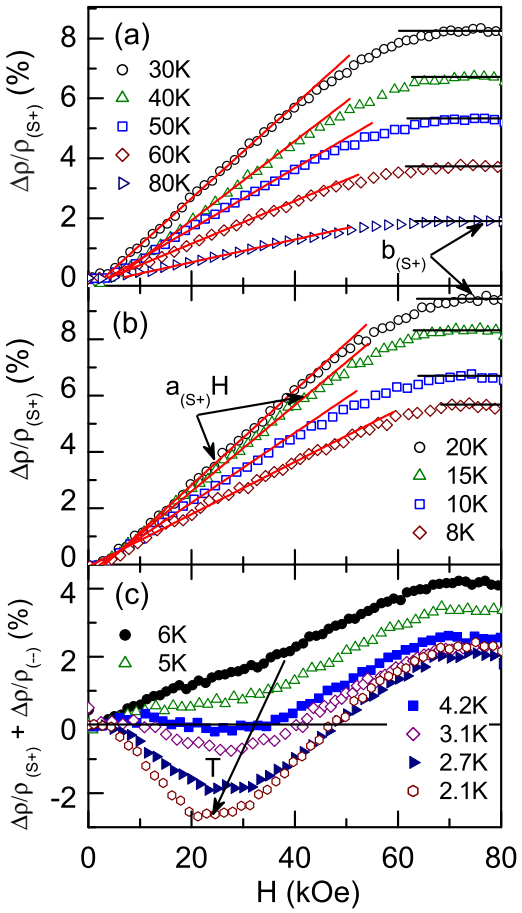


FIG. 9. (Color online) The field dependencies of (a), (b) $\Delta\rho/\rho_{(S+)}$ and (c) $\Delta\rho/\rho_{(S+)} + \Delta\rho/\rho_{(-)}$ contributions to MR of $Ho_{0.1}Lu_{0.9}B_{12}$ compound. The solid lines correspond to the positive linear $a_{(S+)}H$ (red) and saturated $b_{(S+)}$ (black) components of MR term $\Delta\rho/\rho_{(S+)}$, respectively.

that exponents $\alpha_D$ and $\alpha_H$ in dependencies $\mu_D(T) \sim T^{-\alpha_D}$ and $\mu_H(T) \sim T^{-\alpha_H}$ obtained at intermediate temperatures $T \geqslant T^{\star} \sim 60$ K are about equal in the studied compounds [$\alpha_D(x = 0.1) \approx \alpha_H(x = 0.1) \approx 1.6$–$1.7$ and $\alpha_D(x = 0.5) \approx \alpha_H(x = 0.5) \approx 1.3$; see Fig. 10]. The deduced temperature dependencies of coefficient $a_{(s+)}$ and the saturation value $b_{(s+)}$ of the $\Delta\rho/\rho_{(s+)}$ contribution of all compounds (see Fig. S3 in the Supplemental Material [69]) are also similar and connect the slope of the linear increase of MR with the amplitude of the second positive MR component of $Ho_xLu_{1-x}B_{12}$ solid solutions.

### B. Negative magnetoresistance in the paramagnetic phase of $Ho_xLu_{1-x}B_{12}$

Apart from looking for the physical meaning of the second $\Delta\rho/\rho_{(s+)}$ component, it should be stressed that the simple phenomenological procedure applied above for evaluating the positive MR may be developed successfully also to separate the negative magnetoresistance observed for $Ho_xLu_{1-x}B_{12}$ with $x \geqslant 0.1$ at low temperatures. Indeed, on the contrary to the dilute compound with $x = 0.01$ where the only two positive MR components with coefficients $\mu_D$ and $a_{(s+)}$, $b_{(s+)}$ have been observed in a wide temperature range 1.9–120 K (see Fig. 10(a) and Fig. S3 in the Supplemental Material [69]), for magnetic dodecaborides $Ho_xLu_{1-x}B_{12}$ with $x \geqslant 0.1$ the emergence of additional negative magnetoresistance is evident at low temperatures $T < 10$ K, and its amplitude increases dramatically with temperature lowering [see Figs. 9(c) and 11(a)–11(b)]. Moreover, in $Ho_xLu_{1-x}B_{12}$ solid solutions the increase of Ho content is accompanied by a strong increase of the negative MR contribution, e.g., between $\Delta\rho/\rho_{(-)}(x = 0.1) \sim 3\%$ [Fig. 9(c)] and $\Delta\rho/\rho_{(-)}(x = 0.5) \sim 30\%$ [Fig. 11(b)]. A comparative analysis of data presented in Figs. 9(c) and 11 allows us to conclude that (i) at low magnetic field the negative MR follows a quadratic dependence $-\Delta\rho/\rho_{(-)} \sim H^2$ and (ii) that the $\Delta\rho/\rho_{(-)}$ term demonstrates also a tendency to saturation in high magnetic fields. It should be mentioned that such kind of behavior of $\Delta\rho/\rho_{(-)}$ is well known for manganites [49], nonmagnetic and AF heavy-fermion compounds such as $CeCu_6$, $CeAl_3$ [50] and $CeAl_2$, $CeB_6$ [34,35], and AF metal GdSi [32]. Recently this effect has been observed also in dodecaborides $HoB_{12}$, $ErB_{12}$, and $TmB_{12}$ [41] and hexaborides $PrB_6$, $NdB_6$, and $GdB_6$ [52,53], and it was analyzed successfully within the framework of the Yosida approach [54] based on the *s-d* exchange model. This model describes the scattering of charge carries on localized magnetic moments (LMMs) by the relationship between negative MR and local magnetization $\mathbf{M}_{\rm loc}$,

$$-\Delta\rho/\rho_{(-)} \sim M^2_{\rm loc}. \quad (1)$$

In small magnetic fields, where the linear dependence $\mathbf{M}_{\rm loc} \sim \chi_{\rm loc}\mathbf{H}$ is valid, the relationship (1) allows one to explain a simple quadratic field dependence of negative magnetoresistance. Moreover, it was shown in [50,52–53] that the behavior of local magnetic susceptibility $\chi_{\rm loc}(T)$ may be detected directly from the study of the $\Delta\rho/\rho_{(-)}$ term. The emergence of strong negative MR in heavy-fermion compounds was attributed [34,35,50] to a formation of spin-polaron resonance in the electron density of states (DOS) at $E_F$, which appears in systems with strong local $4f$-$5d$ spin fluctuations. Simultaneous polarization of $R^{3+}$ magnetic moments of rare-earth ions and of the spins of conduction electrons in external magnetic field destroys the DOS resonance and prevents the on-site spin-flip scattering.

Taking into account the formation of nanosize magnetic clusters of holmium ions in the dodecaboride matrix [see Figs. 1(e), 1(f)], it is natural to expect that the Langevin function $L(\alpha) = cth(\alpha) - 1/\alpha$ (where $\alpha = \mu_{\rm eff}H/k_BT$; $k_B$ is the Boltzmann constant and $\mu_{\rm eff}$ the effective magnetic moment of the magnetic nanodomains) should provide an appropriate approximation of the local magnetization behavior. As a result, the sum of three terms $\Delta\rho/\rho_{(m+)} = \mu_D^2H^2$, $\Delta\rho/\rho_{(s+)} = (a_{(s+)}H; b_{(s+)})$, and $\Delta\rho/\rho_{(-)} = kL^2(\alpha)$ was taken to fit the magnetoresistance at $T < 10$ K in the paramagnetic phase of $Ho_xLu_{1-x}B_{12}$ solid solutions. In the first step of the procedure the coefficient $\mu_D$ was received directly from the approximation of high-field experimental data $\Delta\rho/\rho(H,T_0)$ [see, e.g., Figs. 5(b), 5(d), and 6(a)]. Parameters $a_{(s+)}(T)$, $b_{(s+)}(T)$, and $\mu_{\rm eff}(T)$ have been deduced from the analysis of residual MR data. For example, Figs. 12(a) and 12(b) show the received contributions to magnetoresistance, $\mu_D^2H^2$, $\Delta\rho/\rho_{(s+)}$, and $kL^2(H/T_0)$ simultaneously with the

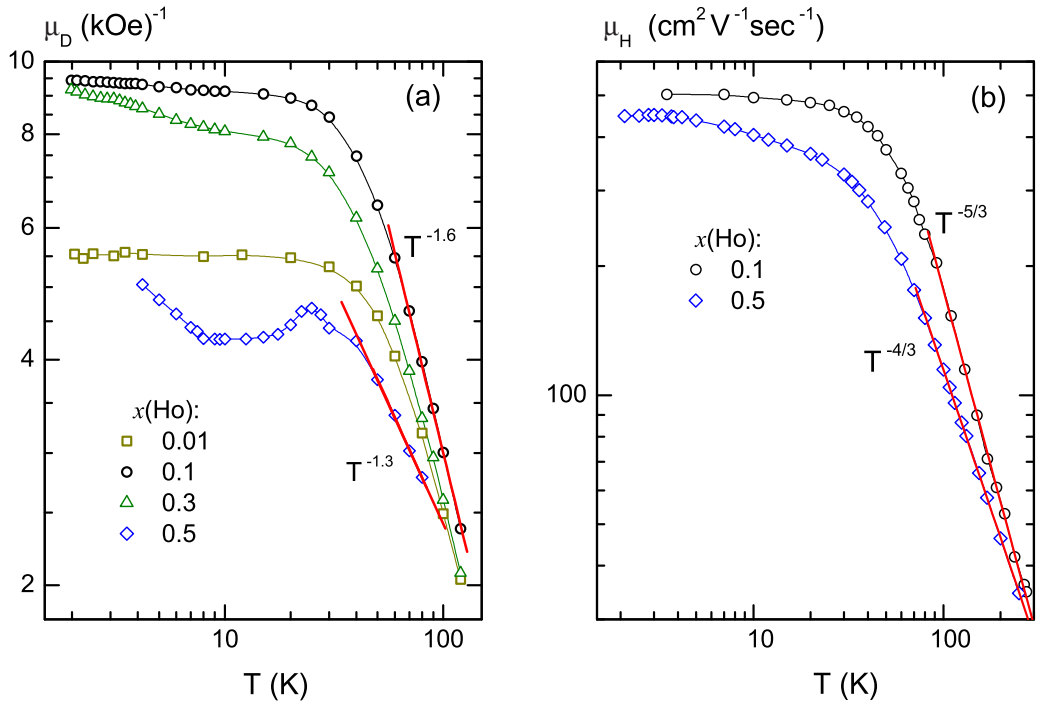


FIG. 10. (Color online) The temperature dependencies of (a) the reduced drift mobility of charge carriers $\mu_D(T)$ and (b) Hall mobility $\mu_H(T) = R_H(T)/\rho(T)$ of solid solutions $Ho_xLu_{1-x}B_{12}$ with $x = 0.01, 0.1, 0.3$, and 0.5 (squares, circles, triangles, and diamonds, respectively). The solid lines on both panels represent the data approximation by the power law $\mu \sim T^{-\alpha}$ (see the text).

experimental curves of $\Delta\rho/\rho(H,T_0)$ recorded at $T \sim 2$ K for $x = 0.1$ and $x = 0.3$, respectively.

Parameters $\mu_{\text{eff}}(T,x)$ and $\chi^{-1}_{\text{loc}}(T,x_0)$ obtained in the framework of this approach are presented in Figs. 13 and 14(a), correspondingly. For comparison, panel (b) of Fig. 14 displays also reciprocal bulk magnetic susceptibility data $\chi^{-1}(T,x_0)$ recorded for the same $Ho_xLu_{1-x}B_{12}$ crystals. It is worth noting that the reduced local susceptibility $\chi_{\text{loc}}(T,x_0) = (1/H)[d(-\Delta\rho/\rho)/dH]^{-1/2}$ was deduced directly from small-field ($H < 5$ kOe) MR data $\Delta\rho/\rho_{\text{exper}} - \Delta\rho/\rho_{(m+)}$, and the parameter $\mu_{\text{eff}}(T,x)$ was independently determined by fitting of the sum $\Delta\rho/\rho_{(s+)} + \Delta\rho/\rho_{(-)}$ [see Figs. 9(c), 11(a), 11(b) in two magnetic field ranges 10–40 kOe and 60–80 kOe].

For the system with nanosize magnetic clusters arranged from the holmium ions [see Figs. 1(e), 1(f)] it is natural to expect a noticeable reduction of $\mu_{\text{eff}}$ values in comparison with $Ho^{3+}$ magnetic moment $\mu(Ho^{3+}) = 10.6\ \mu_B$. Indeed, these small-size clusters with AF exchange interaction inside them may be considered as nanoscale magnetic domains with AF short-range order. In these terms the small-size clusters of $Ho^{3+}$ ions with reduced LMM values should be treated as classical magnetic moments with effective moment $\mu_{\text{eff}}$ whose magnetization is described by the Langevin function $L(\alpha) = cth(\alpha) - 1/\alpha$ (where $\alpha = \mu_{\text{eff}}H/k_BT$). A decrease of $\mu_{\text{eff}}$ is observed in this study both (i) with the temperature lowering [Fig. 13(a)] and (ii) with the increase in Ho content [Fig. 13(b)] in $Ho_xLu_{1-x}B_{12}$ solid solutions. Thus, the AF short-range-order formation can be considered as the most adequate interpretation of the effective moment reduction. The Kondo mechanism of charge-carrier scattering cannot be responsible for the negative MR effect in Ho-based dodecaborides, as $Ho^{3+}$ ($4f^{10}$ configuration, $\Gamma_{51}$ triplet ground state) is not a Kondo ion. Moreover, the analysis of magnetoresistance of $HoB_{12}$, $ErB_{12}$, and $TmB_{12}$ undertaken in [41] allows concluding that both spin-polaron and short-range-order effects are responsible for the appearance of negative magnetoresistance in these dodecaborides. So, the reduction of $\mu_{\text{eff}}(T)$ [Fig. 13(a)] and $\mu_{\text{eff}}(x)$ [Fig. 13(b)] in the paramagnetic state of these cage-glass compounds with nanosize magnetic clusters may be attributed directly to the extension of AF domains in the $RB_{12}$ matrix. Moreover, following to the developed approach it becomes possible to interpret also the violation of the Curie-Weiss law $\chi(T) \sim \mu^2_{\text{eff}}/(T - \theta_p)$ observed for all three $\chi_{\text{loc}}(T)$ curves [Fig. 14(a), right axis]. In this way, taking into account the strong reduction of $\mu_{\text{eff}}$ with temperature lowering [Fig. 13(a)] one has to analyze the product $\chi^{-1}_{\text{loc}}(T)\mu^2_{\text{eff}}(T)$ which is expected to follow the Curie-Weiss relation. And indeed, a linear temperature dependence of the product $\chi^{-1}_{\text{loc}}\mu^2_{\text{eff}}$ is observed for $Ho_xLu_{1-x}B_{12}$ crystals with negative MR, $x = 0.1, 0.3$, and 0.5 [see Fig. 14(a), left axis]. Finally, it should be stressed that for concentrated holmium compounds with $x = 0.3$ and $x = 0.5$ we have obtained almost equal values of $\chi^{-1}_{\text{loc}}(T)$ [Fig. 14(a)] and similar values of $\mu_{\text{eff}}(T)$ [Fig. 13(a)]. These results allow us to conclude that these finite-size antiferromagnetic nanodomains are responsible both for the spin-flip scattering as well as for the appearance of negative MR in the magnetic dodecaborides.

### C. Magnetic phase diagram and MR contributions in the AF state of $Ho_{0.5}Lu_{0.5}B_{12}$

As was mentioned above, the MR effect in the AF phase of $Ho_xLu_{1-x}B_{12}$ is quite different from that observed in the

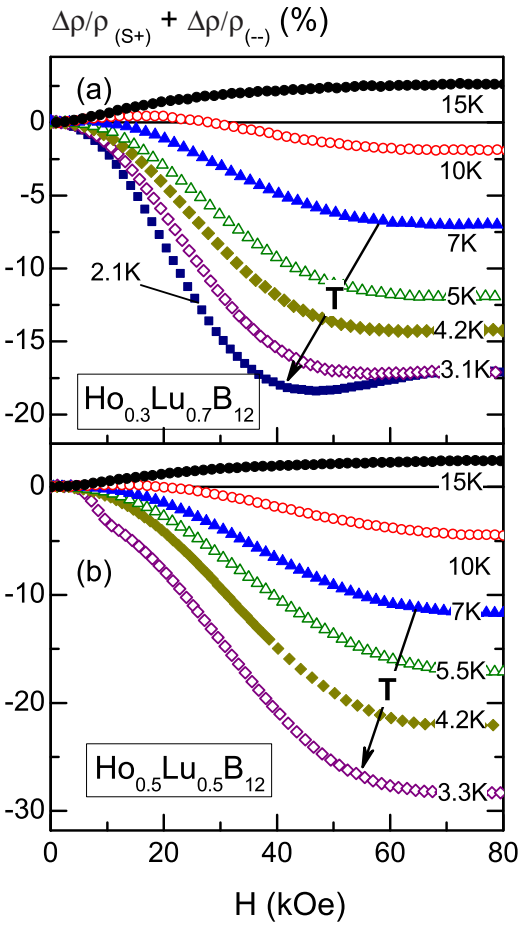


FIG. 11. (Color online) The field dependencies of $\Delta\rho/\rho_{(S+)} + \Delta\rho/\rho_{(-)}$ contribution to MR (see text) for the (a) $Ho_{0.3}Lu_{0.7}B_{12}$ and (b) $Ho_{0.5}Lu_{0.5}B_{12}$ compounds.

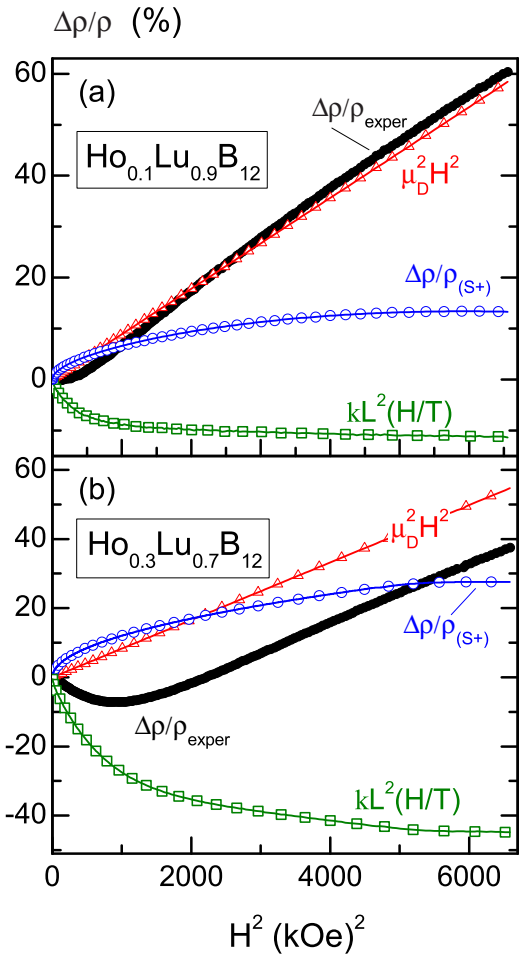


FIG. 12. (Color online) Two examples of MR analysis with contribution separation for the (a) $Ho_{0.1}Lu_{0.9}B_{12}$ and (b) $Ho_{0.3}Lu_{0.7}B_{12}$ compounds at $T_0 = 2$ K. Filled circles correspond to experimental data ($\Delta\rho/\rho_{\text{exper}}$), triangles and open circles to positive contributions $\mu_D^2 H^2$ and $\Delta\rho/\rho_{(S+)}$, and squares to the saturated magnetic component $kL^2(H/T)$.

paramagnetic state. Indeed, at temperatures $T < T_N$ a new large positive magnetoresistance component becomes dominant in moderate magnetic fields, but, in the range $H^{AF}_{\max} < H < H_N$, a strong MR decrease can be seen [Figs. 6(c), 6(d)]. To estimate quantitatively the amplitude of the positive $\Delta\rho/\rho$(AF) term observed in the AF phase we have used an extrapolation of the sum of paramagnetic contributions observed in the P phase in magnetic fields $H < H_N$ [see Fig. 6(c)]; then the $\Delta\rho/\rho$(AF) part can be deduced by subtracting this paramagnetic background from experimental MR data. The obtained AF contribution to MR in $Ho_{0.5}Lu_{0.5}B_{12}$ is shown in Fig. 15. Following the analysis of critical behavior of MR developed in [41], we have calculated also the critical exponent for the amplitude $D_{(AF)}$ of $\Delta\rho/\rho$(AF) (see Fig. 15) in the framework of relation $D_{(AF)} \sim (1 - T/T_N)^{2\beta}$. The exponent $\beta = 0.37 \pm 0.02$ calculated for $Ho_{0.5}Lu_{0.5}B_{12}$ (see inset in Fig. 15) agrees very well with values $\beta = 0.36$ and 0.43 received previously in [41] for $HoB_{12}$, $ErB_{12}$ and $TmB_{12}$, respectively. Within the framework of the Yosida model [54] [see Eq. (1)] a critical behavior of magnetoresistance is expected in the vicinity of $T_N$, and exponents for MR ($\eta$) and for local magnetization ($\beta$) should be connected by relation $\eta = 2\beta$. The critical exponent $\beta = 0.37$ obtained here for $M_{\text{loc}} \sim (-\Delta\rho/\rho)^{1/2}$ is close to values $\beta = 0.335 \pm 0.005$ and $\beta = 0.385 \pm 0.01$ previously observed in magnetization studies of $MnF_2$ and $RbMnF_3$ antiferromagnets [55,56]. In the case of a three-dimensional Heisenberg model the critical exponent of magnetization calculated by expanding into series has a value of $\beta = 0.38 \pm 0.03$, whereas the critical exponent for the three-dimensional Ising model is $\beta = 0.312 \pm 0.005$ [57]. Therefore, the value of $\beta = 0.37$ obtained in this study for the $Ho_{0.5}Lu_{0.5}B_{12}$ magnet is physically justified and, according to our opinion, it can serve as an additional argument in favor of applicability of the spin-polaron approach used here to describe the magnetoresistance of the $Ho_xLu_{1-x}B_{12}$ antiferromagnets. It is also worth noting that the temperature dependence of both the amplitude $I_{AF}$ and the width $\Delta_{AF}$ of magnetic Bragg maxima for the antiferromagnetic phase of the parent $HoB_{12}$ compound was recently investigated in [58] using the neutron diffraction technique. It was revealed that in the vicinity of $T_N$ the parameters $I_{AF}$ and $\Delta_{AF}$ are characterized by a critical behavior with exponents $\beta \approx \gamma \approx 1/3$, which are also in accordance with the critical exponent $\beta \approx 0.37$ received here for $Ho_{0.5}Lu_{0.5}B_{12}$.

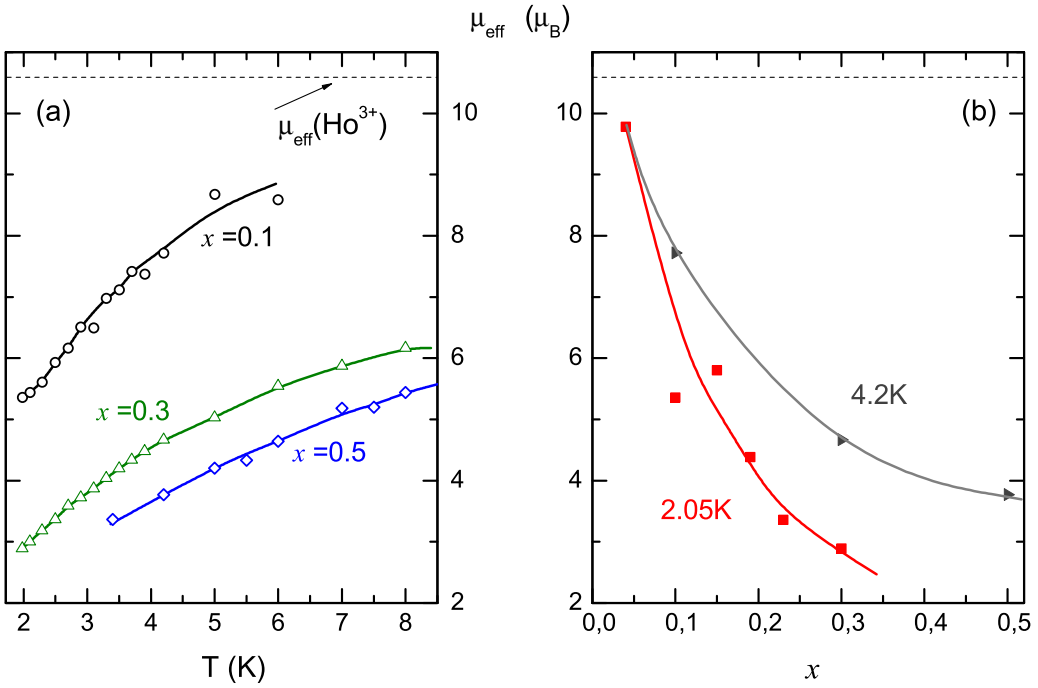


FIG. 13. (Color online) The temperature (a) and the concentration (b) dependencies of effective magnetic moment $\mu_{\text{eff}}$ of $Ho_xLu_{1-x}B_{12}$ with $x \leqslant 0.5$ (see the text). The dashed lines on both panels display the value of effective magnetic moment of $Ho^{3+}$ ion.

To identify precisely the magnetic phase transitions both between AF and P phases and inside the AF state, a numerical differentiation analysis of resistivity curves has been carried out, and features of derivatives $d\rho/dH$ [see Figs. 16(a), 16(b)] were used to construct the *H-T* magnetic phase diagram of $Ho_{0.5}Lu_{0.5}B_{12}$ [see Fig. 16(c)]. The received *H-T* diagram presented in Fig. 16(c) for $Ho_{0.5}Lu_{0.5}B_{12}$ is similar to that observed in [41,48] for parent antiferromagnet $HoB_{12}$ with a higher Néel temperature $T_N \approx 7.4$ K. The high accuracy of resistivity measurements allowed us also to analyze and classify the MR components observed in the $AF_1$ and $AF_2$ phases of the solid solution with $x = 0.5$. Indeed, the analysis of linear fragments of resistivity derivatives [Fig. 16(b)] allows us to describe the magnetoresistance of $Ho_{0.5}Lu_{0.5}B_{12}$ through

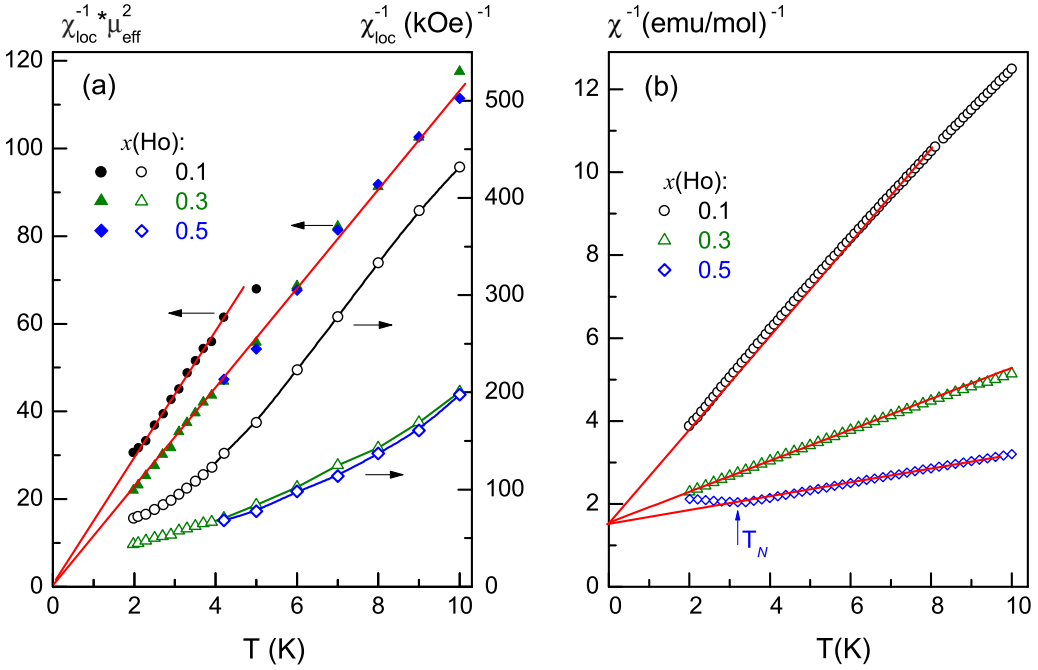


FIG. 14. (Color online) The temperature dependencies of (a) the product $\chi_{\text{loc}}^{-1}\mu_{\text{eff}}^2$ (left axis) and the reciprocal local magnetic susceptibility $\chi_{\text{loc}}^{-1}(T)$ (right axis) and (b) reciprocal bulk magnetic susceptibility $\chi^{-1}(T)$ for $Ho_xLu_{1-x}B_{12}$ solid solutions with $x = 0.1$, 0.3, and 0.5. The solid straight lines show linear approximation.

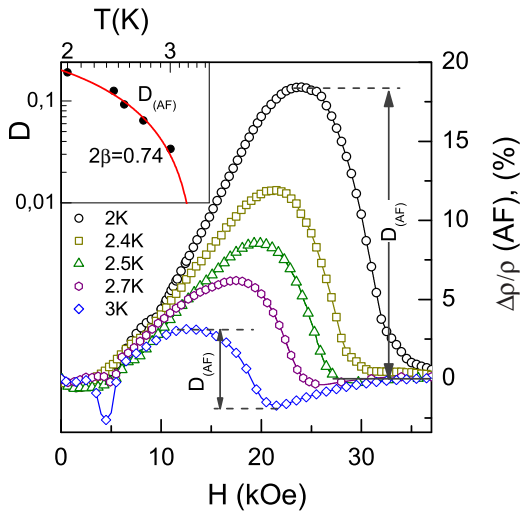


FIG. 15. (Color online) The field dependencies of the $\Delta\rho/\rho$(AF) term of magnetoresistance of $Ho_{0.5}Lu_{0.5}B_{12}$. $D_{AF}$ designates the amplitude of the MR component. The inset shows the result of critical exponent analysis $D_{AF} \sim (1 - T/T_N)^{-2\beta}$ (see the text).

the relationship

$$\Delta\rho/\rho(H,T_0) = -B_{1,2}(T_0)H^2 + A_{1,2}(T_0)H + C. \quad (2)$$

Equation (2) provides us with a good-quality approximation of the MR results both below [phase $AF_1$, $B_1$ and $A_1$ coefficients in Eq. (2)] and above [phase $AF_2$, $B_2$ and $A_2$ coefficients in Eq. (2)] the $T_C(H)$ phase boundary [linear fits for $d\rho/dH$ are shown in Fig. 16(b)]. The calculated temperature dependencies of coefficients $B_{1,2}(T_0)$ and $A_{1,2}(T_0)$ are presented in Figs. 17(a) and 17(b), respectively. As can be seen from Figs. 16(b) and 17(b), simultaneously with the negative quadratic term $\Delta\rho/\rho_{(-)} = -B_{1,2}(T_0)H^2$ a linear positive component $A_{1,2}(T_0)H$ of magnetoresistance appears in the vicinity of $T_N$ in the AF phase of $Ho_{0.5}Lu_{0.5}B_{12}$, and coefficients $A$ and

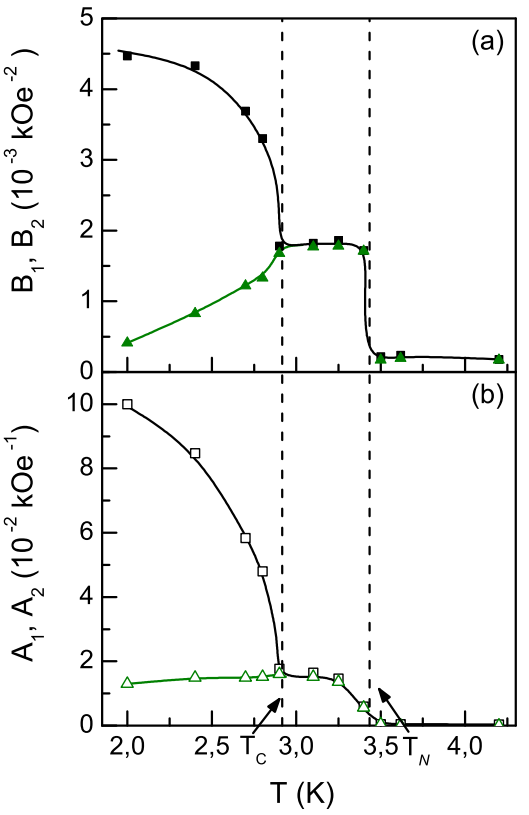


FIG. 17. (Color online) The temperature dependencies of the amplitudes of (a) negative quadratic term ($B_{1,2}$) and (b) linear positive ($A_{1,2}$) component in magnetoresistance of the $Ho_{0.5}Lu_{0.5}B_{12}$ compound [see Eq. (2)].

$B$ change jumpwise in moderate magnetic field 15–25 kOe between ($A_1$, $B_1$) and ($A_2$, $B_2$) values during the $AF_1$-$AF_2$ phase transition observed at $T_C$. Following the arguments presented previously in [41,52,53], the appearance of a linear positive contribution to MR in the antiferromagnetic phase should be

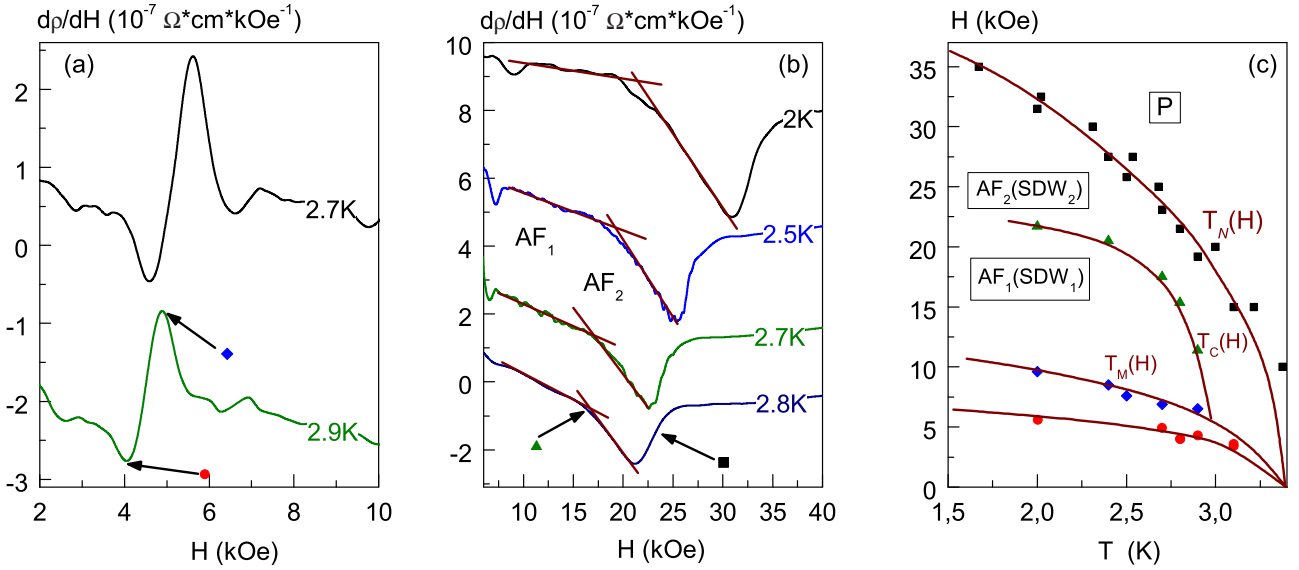


FIG. 16. (Color online) (a), (b) Results of the numerical differentiation of resistivity $d\rho/dH$ in the AF state of the $Ho_{0.5}Lu_{0.5}B_{12}$ compound. The arrows indicate the magnetic phase transitions. (c) $H$-$T$ magnetic phase diagram of $Ho_{0.5}Lu_{0.5}B_{12}$, reconstructed from MR data. Abbreviations: P-paramagnetic state; $AF_{1,2}$ ($SDW_{1,2}$)-antiferromagnetic spin-density wave phases.

attributed to scattering of charge carriers on spin density waves (SDWs). In particular, in the case of metallic chromium which is the most known 3D itinerant antiferromagnet with SDWs (having an incommensurate magnetic structure), the amplitude of linear positive magnetoresistance reaches 180% at magnetic field of $H = 12$ kOe [59]. Similar effects have been found recently [47] in the magnetoresistance of $Tm_{1-x}Yb_xB_{12}$ antiferromagnets with the same modulated incommensurate magnetic structure [$q = (1/2 \pm \delta, 1/2 \pm \delta, 1/2 \pm \delta)$ with $\delta = 0.035$] as in $HoB_{12}$ [58,60]. Thus, according to our analysis, the $AF_1$-$AF_2$ transition observed in $Ho_{0.5}Lu_{0.5}B_{12}$ at $T_C$ [Fig. 16(c)] may be considered as a modification of the spin-density-wave structure, which manifests itself both in (i) changes of the charge-carrier scattering on magnetic nanodomains consisting from interconnected $Ho^{3+}$ ions (expressed by the negative quadratic Langevin type MR component) and (ii) through the increase of the SDW amplitude with increasing magnetic field, resulting in enhancement of charge-carrier scattering on SDWs (expressed through the linear positive MR term). We note that the stabilization and enhancement of SDWs in external magnetic field was predicted previously [61,62]. However, at the same time, to our best knowledge, no theoretical description of charge transport in the presence of an external magnetic field in itinerant magnets with incommensurate SDW structure is available to date, which restricts the possibility of a more detailed microscopic analysis of the positive magnetoresistance effect in the rare-earth dodecaborides.

To summarize the results of this section, we want to discuss below shortly the mechanisms responsible for the emergence of various magnetic phases in the AF state of $Ho_xLu_{1-x}B_{12}$ compounds having a simple face-centered-cubic crystal structure [Figs. 1(a)–1(c)]. To explain the nature of intermediate phases in the AF state of $HoB_{12}$, the authors of [46] proposed a model that considers frustration effects in the fcc lattice of $RB_{12}$. However, when taking into account (i) the loosely bounded state of rare-earth ions in the dodecaboride matrix, (ii) the transition into the cage-glass state of $RB_{12}$ at liquid nitrogen temperatures [39], and (iii) the appearance of disorder in the arrangement of rare-earth ions (random off-site location of $Ho^{3+}$ ions inside the $B_{24}$-truncated cubo-octahedron) resulting in formation of magnetic nanosize clusters in studied compounds, it becomes possible to explain the numerous phase transformations in the AF state as a function of temperature and external magnetic field. Indeed, positional disorder in the arrangement of $Ho^{3+}$ ions in $B_{24}$-truncated cubo-octahedrons leads to a significant dispersion of exchange constants (through indirect exchange, RKKY mechanism). Strong local $4f$-$5d$ spin fluctuations then cause the appearance of an extra factor—the polarization of $5d$ conduction band states (the spin-polaron effect). Moreover, the transition from paramagnetic to AF phase is accompanied by the appearance of induced spin polarization (formation of ferrons, according to the terminology used in [63,64]) and by stabilization of these SDW antinodes in the $RB_{12}$ matrix. The spin-polarized $5d$ component of the magnetic structure (ferrons) is from one side very sensitive to external magnetic field, and, from another side, the applied field suppresses $4f$-$5d$ spin fluctuations by destroying the spin-flip scattering process. Thus, the complex $H$-$T$ phase diagram of $Ho_xLu_{1-x}B_{12}$ magnets may be explained in terms of the formation of a combined magnetically ordered state of localized $4f$ moments of $Ho^{3+}$ ions in combination with spin-polarized local areas of the $5d$ states—ferrons involved in the formation of spin density waves. The presence of the spin polarization was confirmed for $HoB_{12}$ in [46] where a ferromagnetic component of the order parameter was found in the magnetic neutron diffraction patterns. Moreover, even harmonics and hysteresis of the Hall resistance were detected in the range 20 kOe $< H <$ 60 kOe for $HoB_{12}$ and these were attributed to charge-carrier scattering on SDWs [48]. Additional arguments in favor of the SDW component in the magnetic structure of $Ho_xLu_{1-x}B_{12}$ may be found from the results of band structure calculations [65–68]. In particular, a nesting motive between the electron (pancake-like surface centered at the X point) and hole (surface multiply connected in [111] direction) sheets of a Fermi surface (see Fig. S5 in the Supplemental Material [69]) was deduced recently in the studies of Grechnev *et al.* for $HoB_{12}$ [68,70].

## V. CONCLUSIONS

We have studied in detail the transverse magnetoresistance of a model metallic system with a loosely bound state of rare-earth magnetic ions ($Ho^{3+}$) embedded in large-size cavities ($B_{24}$-truncated cubo-octahedrons) of the boron sublattice of $Ho_xLu_{1-x}B_{12}$ substitutional solid solutions. It was shown that positive as well as negative magnetoresistance can be observed in measurements of single crystals of these cage-glass materials. The nMR component which appears in the paramagnetic state of these magnetic metals may be explained in terms of charge-carrier scattering on nanosize clusters of Ho ions with AF exchange and short-range AF order inside these domains. An enhancement of the nMR effect is observed in concentrated Ho-based dodecaborides in the vicinity of Néel temperature, and the Yosida-type relation $-\Delta\rho/\rho \sim M^2$ between magnetoresistance and magnetization is found to provide an adequate description of this term if a Langevin-type behavior of magnetization is present. Moreover, a reduction of effective values of Ho-ion magnetic moments in the range 3–9 $\mu_B$ was found to develop both with temperature lowering and under increase of holmium content. It was shown in the MR analysis that the positive quadratic term $\Delta\rho/\rho_{(m+)} = \mu_D^2 H^2$ dominates for all solid solutions of $Ho_xLu_{1-x}B_{12}$ at intermediate temperatures 20–120 K in strong magnetic fields, allowing us to estimate the exponential behavior of drift mobility of charge carriers $\mu_D \sim T^{-\alpha}$ ($\alpha = 1.3$–$1.7$). In the AF state an additional positive linear MR contribution $\Delta\rho/\rho \sim A(T)H$ was found and it was attributed to charge-carrier scattering on SDW in the incommensurate magnetic structure of these unusual antiferromagnets. In accordance with magnetic-field-induced modification of the AF state which has been observed recently in neutron scattering studies of $HoB_{12}$ [46] we argue in favor of a $SDW_1$-$SDW_2$ magnetic phase transition in $Ho_{0.5}Lu_{0.5}B_{12}$ in external fields of 10–25 kOe. The presented comprehensive MR analysis allows us to reconstruct the $H$-$T$ magnetic phase diagram of $Ho_{0.5}Lu_{0.5}B_{12}$, and provide arguments in favor of a superposition of two components, the $4f$ (based on $Ho^{3+}$ localized moments) and the itinerant $5d$ (based on SDWs) parts, which form the complex magnetic structure of $Ho_xLu_{1-x}B_{12}$ antiferromagnets.

**ACKNOWLEDGMENTS**

We would like to thank V. V. Moshchalkov, A. V. Kuznetsov, G. E. Grechnev, J. Stankiewicz, and K. Siemensmeyer for numerous helpful discussions. This study was supported by the Branch of Physical Sciences of the Russian Academy of Sciences within the program "Strongly Correlated Electrons in Semiconductors, Metals, Superconductors, and Magnetic Materials," Young Scientists Grant of the RF President No. MK-6427.2014.2, and Slovak Scientific Grant Agencies VEGA-2/0106/13 and APVV-0132-11.

[1] W. Thomson, Proc. R. Soc. London **8**, 546 (1856).
[2] C. M. Varma, Phys. Rev. B **54**, 7328 (1996).
[3] P. Majumdar and P. Littlewood, Phys. Rev. Lett. **81**, 1314 (1998).
[4] A. A. Abrikosov, Phys. Rev. B **58**, 2788 (1998).
[5] M. M. Parish and P. B. Littlewood, Phys. Rev. B **72**, 094417 (2005).
[6] J. Hu, M. M. Parish, and T. F. Rosenbaum, Phys. Rev. B **75**, 214203 (2007).
[7] V. B. Shenoy, T. Gupta, H. R. Krishnamurthy, and T. V. Ramakrishnan, Phys. Rev. B **80**, 125121 (2009).
[8] D. I. Golosov, Phys. Rev. Lett. **104**, 207207 (2010).
[9] N. V. Kozlova, N. Mori, O. Makarovsky, L. Eaves, Q. D. Zhuang, A. Krier, and A. Patane, Nat. Commun. **3**, 1097 (2012).
[10] N. J. Harmon and M. E. Flatte, Phys. Rev. Lett. **108**, 186602 (2012).
[11] F. L. Bloom, W. Wagemans, M. Kemerink, and B. Koopmans, Phys. Rev. Lett. **99**, 257201 (2007).
[12] Yu. Wang and J. J. Santiago-Avilés, Appl. Phys. Lett. **89**, 123119 (2006).
[13] B. R. Matis, F. A. Bulat, A. L. Friedman, B. H. Houston, and J. W. Baldwin, Phys. Rev. B **85**, 195437 (2012).
[14] X. Hong, S.-H. Cheng, C. Herding, and J. Zhu, Phys. Rev. B **83**, 085410 (2011).
[15] F. Hellman, M. Q. Tran, A. E. Gebala, E. M. Wilcox, and R. C. Dynes, Phys. Rev. Lett. **77**, 4652 (1996).
[16] S. D. Ganichev, H. Ketterl, W. Prettl, I. A. Merkulov, V. I. Perel, I. N. Yassievich, and A. V. Malyshev, Phys. Rev. B **63**, 201204(R) (2001).
[17] T. A. Dauzhenka, V. K. Ksenevich, I. A. Bashmakov, and J. Galibert, Phys. Rev. B **83**, 165309 (2011).
[18] R. Xu, A. Husmann, T. F. Rosenbaum, M.-L. Saboungi, J. E. Enderby, and P. B. Littlewood, Nature (London) **390**, 57 (1997).
[19] A. Husmann, J. B. Betts, G. S. Boebinger, A. Migliori, T. F. Rosenbaum, and M.-L. Saboungi, Nature (London) **417**, 421 (2002).
[20] T. Thio, S. A. Solin, J. W. Bennett, D. R. Hines, M. Kawano, N. Oda, and M. Sano, Phys. Rev. B **57**, 12239 (1998).
[21] P. Allia, M. Coisson, V. Selvaggini, P. Tiberto, and F. Vinai, J. Magn. Magn. Mater. **262**, 39 (2003).
[22] G. A. Prinz, Science **282**, 1660 (1998).
[23] S. Jin, T. H. Tiefel, M. McCormack, R. A. Fastnacht, R. Ramesh, and L. H. Chen, Science **264**, 413 (1994).
[24] E. Dagotto, T. Hotta, and A. Moreo, Phys. Rep. **344**, 1 (2001).
[25] G. Briceño, H. Chang, X. Sun, P. G. Shultz, and X.-D. Xiang, Science **270**, 273 (1995).
[26] K.-I. Kobayashi, T. Kimura, H. Sawada, K. Terakura, and Y. Tokura, Nature (London) **395**, 677 (1998).
[27] S. Süllow, I. Prasad, S. Bogdanovich, M. C. Aronson, J. L. Sarrao, and Z. Fisk, J. Appl. Phys. **87**, 5591 (2000).
[28] N. Y. Shimakawa, Y. Kubo, and T. Manako, Nature (London) **379**, 53 (1996).
[29] V. A. Gavrichkov, N. B. Ivanova, S. G. Ovchinnikov, T. G. Aminov, A. D. Balaev, G. G. Shabunina, V. K. Chernov, and M. V. Petukhov, Phys. Solid State **41**, 1652 (1999).
[30] S. Weber, P. Lunkenheimer, R. Fichtl, J. Hemberger, V. Tsurkan, and A. Loidl, Phys. Rev. Lett. **96**, 157202 (2006).
[31] S. M. Watts, S. Wirth, S. von Molnar, A. Barry, and J. M. D. Coey, Phys. Rev. B **61**, 9621 (2000).
[32] H. Li, Y. Xiao, B. Schmitz, J. Persson, W. Schmidt, P. Meuffels, G. Roth, and Th. Brückel, Sci. Rep. **2**, 750 (2012).
[33] S. V. Demishev, V. V. Glushkov, I. I. Lobanova, M. A. Anisimov, V. Yu. Ivanov, T. V. Ishchenko, M. S. Karasev, N. A. Samarin, N. E. Sluchanko, V. M. Zimin, and A. V. Semeno, Phys. Rev. B **85**, 045131 (2012).
[34] N. E. Sluchanko, A. V. Bogach, V. V. Glushkov, S. V. Demishev, V. Yu. Ivanov, M. I. Ignatov, A. V. Kuznetsov, N. A. Samarin, A. V. Semeno, and N. Yu. Shitsevalova, JETP **104**, 120 (2007).
[35] A. V. Bogach, G. S. Burkhanov, O. D. Chistyakov, V. V. Glushkov, S. V. Demishev, N. A. Samarin, Yu. B. Paderno, N. Yu. Shitsevalova, and N. E. Sluchanko, Physica B **378-380**, 769 (2006).
[36] J. Y. Chan, S. M. Kauzlarich, P. Klavins, R. N. Shelton, and D. J. Webb, Phys. Rev. B **57**, R8103(R) (1998).
[37] M. B. Salamon, P. Lin, and S. H. Chun, Phys. Rev. Lett. **88**, 197203 (2002).
[38] N. E. Sluchanko, A. N. Azarevich, A. V. Bogach, V. V. Glushkov, S. V. Demishev, A. V. Kuznetsov, K. S. Lyubshov, V. B. Filippov, and N. Yu. Shitsevalova, JETP **111**, 279 (2010).
[39] N. E. Sluchanko, A. N. Azarevich, A. V. Bogach, I. I. Vlasov, V. V. Glushkov, S. V. Demishev, A. A. Maksimov, I. I. Tartakovskii, E. V. Filatov, K. Flachbart, S. Gabáni, V. B. Filippov, N. Yu. Shitsevalova, and V. V. Moshchalkov, JETP **113**, 468 (2011).
[40] N. Sluchanko, S. Gavrilkin, K. Mitsen, A. Kuznetsov, I. Sannikov, V. Glushkov, S. Demishev, A. Azarevich, A. Bogach, A. Lyashenko, A. Dukhnenko, V. Filipov, S. Gabáni, K. Flachbart, J. Vanacken, Gufei Zhang, and V. Moshchalkov, J. Supercond Nov. Magn. **26**, 1663 (2013).
[41] N. E. Sluchanko, A. V. Bogach, V. V. Glushkov, S. V. Demishev, N. A. Samarin, D. N. Sluchanko, A. V. Dukhnenko, and A. V. Levchenko, JETP **108**, 668 (2009).
[42] S. Gabáni, I. Bat'ko, M. Bat'ková, K. Flachbart, E. Gažo, M. Reiffers, N. Shitsevalova, K. Siemensmeyer, and N. Sluchanko, Solid State Sci. **14**, 1722 (2012).
[43] S. Gabáni, E. Gažo, G. Pristáš, I. Takáčová, K. Flachbart, N. Shitsevalova, K. Siemensmeyer, and N. Sluchanko, J. Korean Phys. Soc. **62**, 1514 (2013).
[44] Yu. Paderno, V. Filippov, and N. Shitsevalova, in *Boron-Rich Solids: Albuquerque, NM, 1990*, edited by D. Emin and T. L. Aselage, AIP Conf. Proc., Vol. 231 (American Institute of Physics, New York, 1991), p. 460.

[45] D. L. Strandburg, S. Legvold, and F. H. Spedding, Phys. Rev. **127**, 2046 (1962).
[46] K. Siemensmeyer, K. Babicht, Th. Lonkai, S. Mat'aš, S. Gabáni, N. Shitsevalova, E. Wulf, and K. Flachbart, J. Low Temp. Phys. **146**, 581 (2007).
[47] N. E. Sluchanko, A. N. Azarevich, A. V. Bogach, V. V. Glushkov, S. V. Demishev, A. V. Levchenko, V. B. Filippov, and N. Yu. Shitsevalova, JETP **116**, 866 (2013).
[48] N. E. Sluchanko, D. N. Sluchanko, V. V. Glushkov, S. V. Demishev, N. A. Samarin, and N. Yu. Shitsevalova, JETP Lett. **86**, 604 (2008).
[49] P. Wagner, I. Gordon, L. Trappeniers, J. Vanacken, F. Herlach, V. V. Moshchalkov, and Y. Bruynseraede, Phys. Rev. Lett. **81**, 3980 (1998).
[50] N. E. Sluchanko, A. V. Bogach, G. S. Burkhanov, O. D. Chistyakov, V. V. Glushkov, S. V. Demishev, N. A. Samarin, and D. N. Sluchanko, Physica B **359-361C**, 308 (2005).
[51] A. P. Menushenkov, A. A. Yaroslavtsev, I. A. Zaluzhnyy, A. V. Kuznetsov, R. V. Chernikov, N. Yu. Shitsevalova, V. B. Filippov, JETP Lett. **98**, 165 (2013).
[52] M. A. Anisimov, A. V. Bogach, V. V. Glushkov, S. V. Demishev, N. A. Samarin, V. B. Filipov, N. Yu. Shitsevalova, A. V. Kuznetsov, and N. E. Sluchanko, JETP **109**, 815 (2009).
[53] M. A. Anisimov, A. V. Bogach, V. V. Glushkov, S. V. Demishev, N. A. Samarin, N. Yu. Shitsevalova, A. V. Levchenko, V. B. Filipov, A. V. Kuznetsov, and N. E. Sluchanko, J. Phys. Conf. Ser. **400**, 032003 (2012).
[54] K. Yosida, Phys. Rev. **107**, 396 (1957).
[55] P. Heller, Phys. Rev. **146**, 403 (1966).
[56] A. Sabba Stefanescu and P.-J. Becker, J. Phys. C **14**, L737 (1981).
[57] S. Ma, *Modern Theory of Critical Phenomena* (Benjamin, Reading, MA, 1976).
[58] K. Flachbart, P. Alekseev, G. Grechnev, N. Shitsevalova, K. Siemensmeyer, N. Sluchanko, and O. Zogal, in *Rare Earths: Research and Applications*, edited by K. N. Delfrey (Nova Science, Hauppauge, NY, 2008), Chap. 2, pp. 79-125.
[59] S. Arajs and G. R. Dunmyre, J. Appl. Phys. **36**, 3555 (1965).
[60] K. Siemensmeyer, K. Flachbart, S. Gabáni, S. Mat'aš, Y. Paderno, and N. Shitsevalova, J. Solid State Chem. **179**, 2748 (2006).
[61] T. Sasaki, A. G. Lebed, T. Fukase, and N. Toyota, Phys. Rev. B **54**, 12969 (1996).
[62] G. Montambaux, Phys. Rev. B **38**, 4788 (1988).
[63] E. L. Nagaev, JETP Lett. **6**, 18 (1967).
[64] M. Yu. Kagan, K. I. Kugel, and D. I. Khomskii, JETP **93**, 415 (2001).
[65] M. Heinecke, K. Winzer, J. Noffke, H. Kranefeld, H. Grieb, K. Flachbart, and Yu. B. Paderno, Z. Phys. B **98**, 231 (1995).
[66] N. Okuda, T. Suzuki, I. Ishii, S. Hiura, F. Iga, T. Takabatake, T. Fujita, H. Kadomatsu, and H. Harima, Physica B **281-282**, 756 (2000).
[67] B. Jager, S. Paluch, O. J. Zogal, W. Wolf, P. Herzig, V. B. Filippov, N. Shitsevalova, and Y. Paderno, J. Phys. Condens. Matter **18**, 2525 (2006).
[68] A. E. Baranovskiy, G. E. Grechnev, N. Yu. Shitsevalova, D. N. Sluchanko, V. V. Glushkov, S. V. Demishev, and N. E. Sluchanko, Low Temp. Phys. **35**, 565 (2009).
[69] See Supplemental Material at http://link.aps.org/supplemental/10.1103/PhysRevB.91.235104 for more information (X-ray Laue-patterns and lattice constant changes with Ho content [Fig. S1]; derivatives of magnetoresistance [Fig. S2]; temperature dependencies $a_{(S+)}$ and $b_{(S+)}$ coefficients [Fig. S3]; band structure [Fig. S4] and Fermi surface [Fig. S5] of $LuB_{12}$; temperature dependencies of resistivity and Hall coefficient in vicinity of Néel temperature in comparison with chromium data [Fig. S6]; heat capacity $C(T)$ and $T_N(x)$ in $Ho_xLu_{1-x}B_{12}$ [Fig. S7]; variation of effective moment with the temperature $\mu_{\text{eff}}(T)$ [Fig. S8]).
[70] G. E. Grechnev (private communication).